

Revisiting the Jaynes–Cummings model with time-dependent coupling

Thiago T. Tsutsui^{1,*}, Danilo Cius^{2,†}, Antonio Vidiella-Barranco^{3,‡},
Antonio S. M. de Castro^{1,4,§} and Fabiano M. Andrade^{1,5,¶}

¹Programa de Pós-Graduação em Ciências/Física, Universidade Estadual de Ponta Grossa, 84030-900 Ponta Grossa, Paraná, Brazil

²Instituto de Física, Universidade de São Paulo, 05508-090 São Paulo, São Paulo, Brazil

³Instituto de Física "Gleb Wataghin", Universidade de Campinas, 13083-859, Campinas, São Paulo, Brazil

⁴Departamento de Física, Universidade Estadual de Ponta Grossa 84030-900 Ponta Grossa, Paraná, Brazil

⁵Departamento de Matemática e Estatística, Universidade Estadual de Ponta Grossa, 84030-900 Ponta Grossa, Paraná, Brasil

(Dated: August 28, 2025)

The Jaynes–Cummings (JC) model stands as a fully quantized, fundamental framework for exploring light–matter interactions, a timely reflection on a century of quantum theory. The time-dependent Jaynes–Cummings (TDJC) model introduces temporal variations in certain parameters, which often require numerical methods. However, under the resonance condition, exact solutions can be obtained, offering insight into a variety of physical scenarios. In this work, we study the resonant TDJC model considering different modulations of the atom–field coupling. The model is presented and an analytical solution derived in a didactic way, allowing us to examine how time-dependent couplings affect atomic population inversion and atom–field entanglement. We also consider an atom traversing a partially cooled cavity, which induces periodicity and reveals the combined effects of atomic motion and thermal fluctuations. The Bloch vector is used to analyze the dynamics of the system, including the atomic state purity, and reveals phenomena such as atomic dipole alignment with the field due to the oscillating coupling, as well as atomic population trapping, which arises by increasing the initial mean thermal photon number.

I. INTRODUCTION

In 2025, we mark the centenary of the inception of quantum mechanics, a revolutionary theory that continues to drive progress through the ongoing development of quantum technologies. The birth of quantum theory is deeply connected to the investigation of electromagnetic (EM) radiation and atoms, which remain central to both foundational investigations and emerging applications. More recently, the development of the laser, a coherent light source, gave rise to the subfield of nonrelativistic quantum electrodynamics theory known as quantum optics, which basically explores the nature and effects of quantized light. In this context, the most elementary quantum model of light–matter interaction consists of a highly idealized atom (modeled as a two-level system) coupled to a single mode of the quantized EM field. Under the rotating wave approximation (RWA), this model, known as the Jaynes–Cummings (JC) model [1, 2], remarkably admits an exact analytical solution, and despite the simplifying assumptions underlying its construction [3], the JC model provides deep insights into several fundamental aspects of light–matter interaction. Originally developed to compare semiclassical and quantum approaches to spontaneous emission [4], the JC model has since evolved to uncover nonclassical phenomena such as the experimentally observed collapses [5] and revivals of the Rabi oscillations (RO) [6–10], squeezing [11, 12], sub-Poissonian statistics [13, 14], atom–field entanglement [15–17], and the generation of Schrödinger cat states [18, 19].

Furthermore, the core of the model is a two-level system (TLS) coupled to a harmonic oscillator, which allows it to be mapped onto trapped ion [20–22] and relativistic systems [23]. Regarding applications, the JC framework is employed in several quantum information processing schemes [24, 25]. There are also generalizations of the model involving additional field modes and atomic levels [26, 27], multiple two-level atoms [28, 29], quantum deformations [30–32], Kerr-like media [33, 34] and external pumpings [35, 36]. Besides, the model naturally extends to the description of open quantum systems, where interaction with the environment leads to dissipation and decoherence [37–39].

A particularly interesting generalization is obtained when the model parameters are allowed to vary in time, giving rise to the time-dependent JC (TDJC) model [24, 40]. This may account for atomic motion [41, 42], transient effects in the cavity [43, 44], or the incorporation of stochastic aspects [45]. However, unlike the standard JC model, analytical methods are not always applicable. Notable exceptions are the Nikitin [43], Rosen-Zener [44], Landau-Zener [46, 47] and Demkov–Kunike [46] models. Remarkably, under the resonance condition, it is possible to obtain exact solutions considering a time-dependent atom–field coupling [41, 42, 48]. From an experimental point of view, Ref. [49] suggests that a time-dependent coupling may be achievable in cavity quantum electrodynamics through variations in the atom’s position or by changing an external electric field.

The objective of this work is twofold: we first present a didactic overview of the solution of the resonant TDJC model in terms of the evolution operator. We discuss two specific cases of time-dependent atom–field coupling: (i) linear [48] and (ii) hyperbolic secant [44]. The latter is particularly desirable in quantum control [50], where manipulating the TLS is one potential objective [51, 52]. We focus on the dynamics of the atomic population inversion and the von Neumann en-

* takajitsutsui@gmail.com

† danilocius@gmail.com

‡ vidiella@ifi.unicamp.br

§ asmcastro@uepg.br

¶ fmandrade@uepg.br

trophy, examining the impact of the time dependence on both quantities. The subsystems are assumed to be initially prepared in pure states, in which case the entropy directly reflects the atom–field entanglement. In the second part of the paper, we consider the atom moving inside the cavity, which leads to a sinusoidal time dependence for the atom–field coupling. Related scenarios have been explored in the literature, particularly in studies of entanglement [53, 54], self-induced transparency effects [41], and the role of atomic coherence in the JC model with motion [55]. We also assume a different set of initial conditions, viz., the field in a thermal state and the atom prepared either in the excited state or in a superposition of atomic ground and excited states (eigenstate of $\hat{\sigma}_x$). The JC model with a partially cooled cavity is relevant, for example, to the study of entanglement [54, 56], and is also experimentally accessible [9]. We analyze the atomic evolution from a different perspective, focusing on the Bloch vector dynamics and compare our results to the established findings [56–59] within the context of constant coupling. We find that the behavior of the studied quantities, basically the components and modulus of the Bloch vector, is generally dominated by the periodic coupling, even in the presence of thermal noise, in contrast to the constant coupling case [56]. We note that a periodic evolution of both the field entropy and the atomic inversion, induced by atomic motion and in the absence of thermal noise, was reported in [42]. Other effects may arise, manifesting in the Bloch vector dynamics. Two control parameters in the system, p , the number of half-wavelengths of the standing-wave cavity, and ζ_3 , proportional to the velocity of the moving atom, have similar effects. For instance, smaller values of p and ζ_3 lead to a dynamical evolution with longer periods, more closely resembling the behavior of the constant-coupling case. Interestingly, increasing the thermal fluctuations, which corresponds to a larger mean photon number in the initial field state, leads to a form of atomic population trapping [57], while the periodicity of the Bloch vector dynamics tends to persist despite the added noise.

We organize the paper as follows. In Sec. II, we provide an overview of the standard JC model, deriving the time-evolution operator and highlighting key aspects of the dynamics. Subsequently, in Sec. III, we examine the effects of a time-dependent coupling parameter on both the population inversion and atom–field entanglement, presenting a general time-evolution operator for this case and analyzing two types of modulations. Having established the appropriate formalism, we consider the case of an atom moving across a partially cooled cavity, focusing on the combined impact of sinusoidal coupling and thermal fluctuations on the Bloch vector dynamics. Finally, our conclusions are summarized in Sec. V.

II. JAYNES-CUMMINGS MODEL

The JC model is the simplest fully quantum description of light–matter interaction [60]. In the JC framework, matter is represented by one atom, associated with a single atomic transition, while light is embodied as a quantized mode of the EM field. To address this problem, we consider that the Hamil-

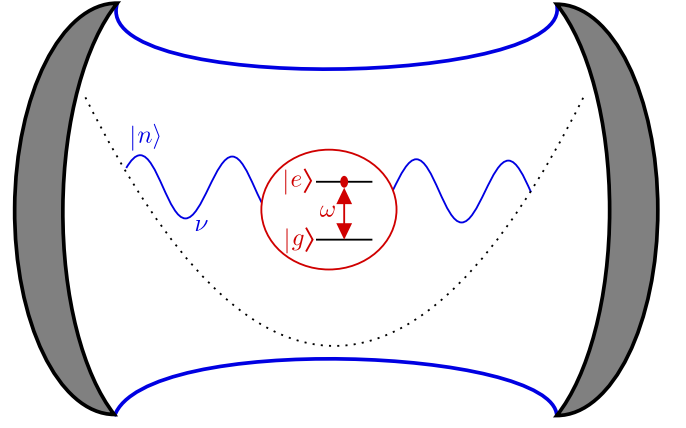


FIG. 1. A schematic description of the JC model. The atom is represented as a TLS, namely $|e\rangle$ and $|g\rangle$, with a transition frequency ω , while the cavity mode is modeled as a simple harmonic oscillator with frequency ν and characterized by the Fock states $|n\rangle$, $n = 0, 1, 2, \dots$

tonian of the system, \hat{H} , consists of three parts: the atomic energy \hat{H}_A , the EM energy \hat{H}_F , and the interaction term \hat{H}_I [61, 62]. The atom is modelled as a TLS, where $|e\rangle$ and $|g\rangle$ denote the excited and ground states, respectively. The field mode, on the other hand, is treated as a simple harmonic oscillator, with the Fock states $|n\rangle$, $n = 0, 1, 2, \dots$, serving as a basis. From the aforementioned concepts and employing the dipole approximation, we derive the quantum Rabi model [63]. Further applying the RWA, we obtain the JC model, whose Hamiltonian is governed by (hereafter we assume $\hbar = 1$)

$$\hat{H} = \frac{1}{2}\omega\hat{\sigma}_z + \nu\hat{a}^\dagger\hat{a} + \lambda(\hat{\sigma}_+\hat{a} + \hat{\sigma}_-\hat{a}^\dagger), \quad (1)$$

where ω and ν denote the frequencies of the atomic transition and cavity mode, respectively, while λ is the coupling parameter, assumed to be real. In Fig. 1, we schematically represent the JC model.

For the TLS, we consider the Pauli matrices $\hat{\sigma}_k$, $k = x, y, z$, where the ladder operators $\hat{\sigma}_\pm = \hat{\sigma}_x \pm i\hat{\sigma}_y$ serve as generators of the $\mathfrak{su}(2)$ algebra [64], satisfying the commutation relation $[\hat{\sigma}_+, \hat{\sigma}_-] = 2\hat{\sigma}_z$. In the atomic basis, we can express the aforementioned operators as $\hat{\sigma}_+ = |e\rangle\langle g|$, $\hat{\sigma}_- = |g\rangle\langle e|$ and $\hat{\sigma}_z = |e\rangle\langle e| - |g\rangle\langle g|$. Conversely, the cavity mode is characterized by the bosonic operators, elements of the Weyl-Heisenberg algebra [65], obeying $[\hat{a}, \hat{a}^\dagger] = 1$. Their action characterizes the creation (annihilation) of quanta: $\hat{a}^\dagger|n\rangle = \sqrt{n+1}|n+1\rangle$ ($\hat{a}|n\rangle = \sqrt{n}|n-1\rangle$).

The JC system is a composite system comprising two subsystems, the TLS and the cavity mode, and is therefore classified as bipartite. The Hilbert space associated with the JC system, \mathcal{H} , is defined as $\mathcal{H} = \mathcal{H}_A \otimes \mathcal{H}_F$, where \mathcal{H}_A represents the atomic Hilbert space with dimension 2, and \mathcal{H}_F corresponds to the cavity Hilbert space, which has infinite dimension. As such, the tensor product is used to denote the composite system state. Given an atomic state $|\psi_A\rangle$, $|\psi_A\rangle \in \mathcal{H}_A$, and a field state $|\psi_F\rangle$, $|\psi_F\rangle \in \mathcal{H}_F$, the initial state

of the system can be in particular expressed as a product state $|\Psi\rangle = |\psi_A\rangle \otimes |\psi_F\rangle = |\psi_A, \psi_F\rangle$, provided these subsystems are initially uncorrelated. In this context, the bare states of the JC model are defined as $|e, n\rangle$ and $|g, n+1\rangle$, which are eigenstates of the excitation number operator [24]

$$\hat{N}_E = \hat{a}^\dagger \hat{a} + \frac{1}{2} \hat{\sigma}_z. \quad (2)$$

It is straightforward to verify that $[\hat{H}, \hat{N}_E] = 0$, confirming that \hat{N}_E is a conserved quantity. This conservation gives rise to a continuous $U(1)$ symmetry, in accordance with Noether's theorem [3], and ultimately enables the exact solution of the system's dynamics. Employing Eq. (2), we can rewrite the Hamiltonian as

$$\hat{H} = \nu \hat{N}_E + \frac{1}{2}(\omega - \nu) \hat{\sigma}_z + \lambda (\hat{\sigma}_+ \hat{a} + \hat{\sigma}_- \hat{a}^\dagger). \quad (3)$$

In the interaction picture relative to the term $\nu \hat{N}_E$ and under the resonance condition ($\omega = \nu$), we obtain the interaction Hamiltonian

$$\hat{V} = \lambda (\hat{\sigma}_+ \hat{a} + \hat{\sigma}_- \hat{a}^\dagger). \quad (4)$$

Choosing a basis that diagonalizes \hat{N}_E results in a block-diagonal structure in the interaction Hamiltonian \hat{V} [66]. Each block $\hat{V}^{(n)}$, corresponds to a specific photon number n and has a 2×2 dimension, due to the degeneracy of the eigenvectors of the excitation number operator, $|e, n\rangle$ and $|g, n+1\rangle$, coupled by the interaction energy expressed in Eq. (4). The ground state $|g, 0\rangle$ is the only eigenstate of \hat{N}_E that is not coupled to another bare state, associated with a 1×1 block and being an eigenvector of the interaction Hamiltonian. Therefore, employing the bare state basis $\{|e, n\rangle, |g, n+1\rangle\}$, we can represent \hat{V} in matrix form as

$$\hat{V} = \begin{bmatrix} 0 & 0 & 0 & \cdots \\ 0 & \hat{V}^{(0)} & 0 & \cdots \\ 0 & 0 & \hat{V}^{(1)} & \cdots \\ \vdots & \vdots & \vdots & \ddots \end{bmatrix}, \quad (5)$$

where

$$\hat{V}^{(n)} = \lambda \sqrt{n+1} \begin{bmatrix} 0 & 1 \\ 1 & 0 \end{bmatrix}. \quad (6)$$

In the matrix, it is possible to observe how the Hamiltonian $\hat{V}^{(n)}$ couples the states within a single 2×2 subspace, with the emission and absorption processes described by the off-diagonal elements: $\langle e, n | \hat{V} | g, n+1 \rangle$ corresponds to the transition $|g, n+1\rangle \rightarrow |e, n\rangle$, while $\langle g, n+1 | \hat{V} | e, n \rangle$ describes $|e, n\rangle \rightarrow |g, n+1\rangle$ [67].

There are several approaches to studying the dynamics of the JC model [68]. In this context, we focus on the time-evolution operator $\hat{U}(t)$, primarily because it provides a smooth transition from the standard to the TDJC model. Considering the interaction Hamiltonian, Eq. (4), the time-evolution operator is defined as [69]

$$\hat{U}(t) = e^{-i\hat{V}t}. \quad (7)$$

We evaluate the exponential employing the series expansion

$$\hat{U}(t) = \sum_{\ell=0}^{\infty} \frac{(-i\hat{V}t)^\ell}{\ell!}. \quad (8)$$

The terms of the expansion can be further decomposed by examining their action on $|e, n\rangle$. Inductively:

$$\begin{aligned} (\hat{V})^{2\ell} |e, n\rangle &= (\lambda)^{2\ell} (n+1)^\ell |e, n\rangle \quad (\text{even}), \\ (\hat{V})^{2\ell+1} |e, n\rangle &= (\lambda)^{2\ell+1} (n+1)^{\ell+1/2} |g, n+1\rangle \quad (\text{odd}). \end{aligned} \quad (9)$$

The action of $(\hat{V})^{2\ell}$ leaves the state unchanged, apart from a multiplicative constant. In contrast, the action of $(\hat{V})^{2\ell+1}$, in addition to the constant, results in the inversion of $|e, n\rangle$. We can extend this analysis to the action on the state $|g, n+1\rangle$, and, subsequently, separate the even and odd terms in the expansion of \hat{V} [16]:

$$\begin{aligned} (\hat{\sigma}_+ \hat{a} + \hat{\sigma}_- \hat{a}^\dagger)^{2\ell} &= (\hat{a} \hat{a}^\dagger)^\ell |e\rangle\langle e| + (\hat{a}^\dagger \hat{a})^\ell |g\rangle\langle g|, \\ (\hat{\sigma}_+ \hat{a} + \hat{\sigma}_- \hat{a}^\dagger)^{2\ell+1} &= (\hat{a} \hat{a}^\dagger)^\ell \hat{a} |e\rangle\langle g| + \hat{a}^\dagger (\hat{a} \hat{a}^\dagger)^\ell |g\rangle\langle e|. \end{aligned} \quad (10)$$

Employing Eq. (10) and algebraic manipulations, we can express $\hat{U}(t)$, in the more convenient form of

$$\begin{aligned} \hat{U}(t) &= \sum_{\ell=0}^{\infty} \left\{ \frac{(-i\lambda t)^{2\ell}}{(2\ell)!} \left[(\sqrt{\hat{a} \hat{a}^\dagger})^{2\ell} |e\rangle\langle e| + (\sqrt{\hat{a}^\dagger \hat{a}})^{2\ell} |g\rangle\langle g| \right] \right. \\ &\quad \left. + \frac{(-i\lambda t)^{2\ell+1}}{(2\ell+1)!} \left[\frac{(\sqrt{\hat{a} \hat{a}^\dagger})^{2\ell+1}}{\sqrt{\hat{a} \hat{a}^\dagger}} \hat{a} |e\rangle\langle g| + \hat{a}^\dagger \frac{(\sqrt{\hat{a} \hat{a}^\dagger})^{2\ell+1}}{\sqrt{\hat{a} \hat{a}^\dagger}} |g\rangle\langle e| \right] \right\}. \end{aligned} \quad (11)$$

By using the series definition of the sine and cosine functions [70], we can express the operator with the closed expression [24]

$$\begin{aligned} \hat{U}(t) &= \cos(\lambda t \sqrt{\hat{a}^\dagger \hat{a} + 1}) |e\rangle\langle e| + \cos(\lambda t \sqrt{\hat{a} \hat{a}^\dagger}) |g\rangle\langle g| \\ &\quad - i \frac{\sin(\lambda t \sqrt{\hat{a}^\dagger \hat{a} + 1})}{\sqrt{\hat{a}^\dagger \hat{a} + 1}} \hat{a} |e\rangle\langle g| - i \hat{a}^\dagger \frac{\sin(\lambda t \sqrt{\hat{a} \hat{a}^\dagger})}{\sqrt{\hat{a} \hat{a}^\dagger}} |g\rangle\langle e|. \end{aligned} \quad (12)$$

Equipped with the time evolution operator $\hat{U}(t)$, we can analyze the system's dynamics. We consider the initial state

$$|\Psi(0)\rangle = |e, \alpha\rangle, \quad (13)$$

where $|\alpha\rangle = \sum_{n=0}^{\infty} C_n |n\rangle$ denotes a coherent state [71]. Coherent states play a fundamental role in quantum optics and in the study of the JC model, as they are minimum-uncertainty states that closely resemble a classical description of the EM field. They have a Poissonian photon number distribution and, unlike nonclassical states such as Fock states, are more readily accessible in experiments [72]. The expansion coefficients are given by

$$C_n = e^{-|\alpha|^2/2} \frac{\alpha^n}{\sqrt{n!}}, \quad (14)$$

where $|\alpha|^2 = \langle n \rangle$ represents the initial average photon number in the cavity.

The system evolves according to $|\Psi(t)\rangle = \hat{U}(t)|\Psi(0)\rangle$, which leads to [61, 62]

$$|\Psi(t)\rangle = \sum_{n=0}^{\infty} [C_{e,n}(t)|e\rangle + C_{g,n}(t)|g\rangle] |n\rangle, \quad (15)$$

where the probability amplitudes are given by

$$\begin{aligned} C_{e,n}(t) &= C_n \cos(2\lambda \sqrt{n+1}t) \\ C_{g,n}(t) &= -iC_{n-1} \sin(2\lambda \sqrt{n}t). \end{aligned} \quad (16)$$

Taking the square modulus of Eq. (16) and marginalizing over the Fock states, we obtain the probabilities of finding the TLS in the excited and ground states, respectively,

$$\begin{aligned} P_e(t) &= \sum_{n=0}^{\infty} |C_{e,n}(t)|^2, \\ P_g(t) &= \sum_{n=0}^{\infty} |C_{g,n}(t)|^2. \end{aligned} \quad (17)$$

In this context, a quantity of interest is the expectation value $W(t) = \langle \hat{\sigma}_z \rangle$, referred to as the population inversion, which can be written as

$$W(t) = P_e(t) - P_g(t). \quad (18)$$

This function is experimentally measurable [24, 73], often computed within the JC model and its extensions [74].

For the initial state $|\Psi(0)\rangle = |e, \alpha\rangle$, the population inversion is

$$W(t) = \sum_{n=0}^{\infty} P_n \cos(2\lambda \sqrt{n+1}t), \quad (19)$$

where $P_n = |C_n|^2$ if the Poissonian photon number distribution of the initial coherent field state $|\alpha\rangle$, with $\langle n \rangle = |\alpha|^2$. The sum of the trigonometric functions, weighted by P_n , results in the collapses and revivals of the RO – a hallmark of the JC model that underscores the quantum signature of the EM field. This phenomenon arises as RO dephase over time due to the spread of the Rabi frequencies caused by the photon number distribution of the coherent state, leading to their “collapse”. Rephasing occurs at later times, causing the oscillations to “revive”, with the first revival occurring approximately at $t_r = 2\pi \sqrt{\langle n \rangle} / \lambda$ [24].

Since the state in Eq. (15) cannot, in general, be written as a product state of the form $|\Psi\rangle = |\psi_A\rangle \otimes |\psi_F\rangle$, it is typically non-separable [51]. This reflects the phenomenon of entanglement, where two or more systems become so strongly correlated that they can no longer be described independently. Mathematically, this arises from the quantum formalism, where the system’s Hilbert space is described using the tensor product of its subsystems Hilbert spaces. Consequently, the resulting state vector is generally not a product of the individual states of the system [75]. Historically, the

investigation of entanglement is deeply intertwined with the development of quantum mechanics. The phenomenon was first explicitly discussed by Schrödinger in 1935, who coined the term entanglement (*verschränkung*) to describe the peculiar quantum correlations between particles [76]. Earlier that same year, Einstein, Podolsky, and Rosen had published their seminal paper [77], which, while not using the term entanglement, highlighted the odd nature of quantum correlations and challenged the completeness of quantum mechanics. Later, in 1964, Bell formulated his famous theorem, which demonstrated that the predictions of quantum mechanics for entangled pure states cannot be explained by any local hidden variable theory, thereby emphasizing the nonlocal nature of quantum entanglement [78].

In this context, for pure states in bipartite systems, the von Neumann entropy [79] provides a well-established measure of entanglement [24, 80]. While the von Neumann entropy quantifies the mixedness of a density matrix in general, when computed for the reduced density matrix of one subsystem, it effectively measures the degree of entanglement between the two subsystems. This occurs because, the more correlated the system is, the less information is retained in the reduced subsystem after the partial trace, leading to a more mixed state.

The Schmidt decomposition [81, 82] is particularly useful when dealing with two subsystems, one of which has dimension m ($m \neq 2$). It guarantees that, for a bipartite system in a pure global state, there exists an orthonormal basis $\{|b_i(t)\rangle, i = 1, 2, 3, \dots\}$ for subsystem B and $\{|c_j(t)\rangle, j = 1, 2, 3, \dots\}$ for subsystem C , such that the state of the system, $|\psi_{BC}\rangle \in \mathcal{H}_{BC}$, can be written as

$$|\psi_{BC}(t)\rangle = \sum_i \mu_i(t) |b_i(t), c_i(t)\rangle. \quad (20)$$

In the expression above, the upper limit of the index i is the *smaller* of the dimensions of the Hilbert spaces involved. In the case of the JC model, for instance, the Schmidt decomposition allows the state vector to be expressed in terms of just two terms—even though the cavity’s Hilbert space is infinite-dimensional. This greatly facilitates the computation of the von Neumann entropy.

The von Neumann entropy is defined as $S_j(t) = -\text{Tr}[\hat{\rho}_j(t) \log_2 \hat{\rho}_j(t)]$, where j denotes the specific subsystem. The maximum entropy value is $\log_2(\dim \mathcal{H}_i)$, and base two is chosen arbitrarily so that the maximum value is 1 when evaluating the subsystems of the JC model. In a basis where $\hat{\rho}_j(t)$ is diagonal with eigenvalues $\mu_i(t)$, the von Neumann entropy is given by

$$S_j(t) = -\sum_i \mu_i(t) \log_2 \mu_i(t). \quad (21)$$

Notably, for pure initial states, the entropies of the reduced subsystems are equal, i.e., $S_B(t) = S_C(t)$ [83], where $j = B, C$ represents generic correlated subsystems [24]. In Fig. 2, we provide a schematic representation of the relationship between the von Neumann entropy and entanglement.

Atom-field entanglement is one of the hallmark nonclassical features of the JC model [16, 17, 80]. Historically, the purity of the state was first studied by Aravind and Hirschfelder

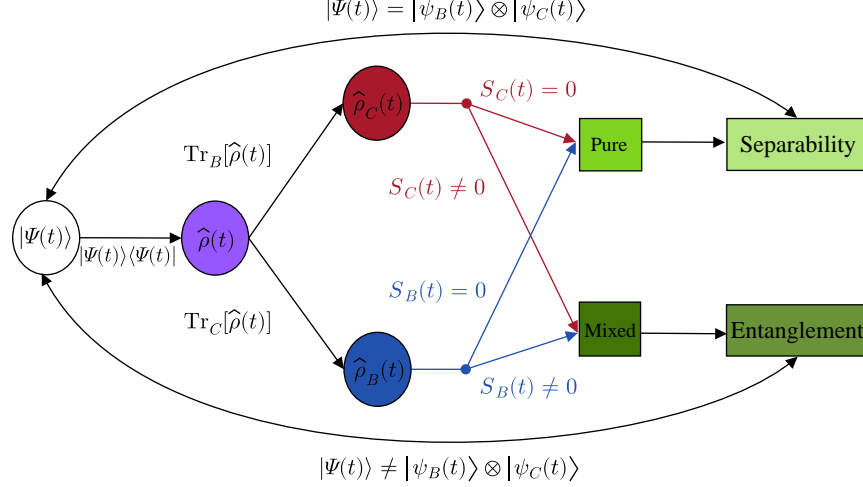


FIG. 2. Scheme for the relation between the von Neumann entropy and entanglement. We begin with an initial pure state $|\Psi(t)\rangle \in \mathcal{H}_{BC} = \mathcal{H}_B \otimes \mathcal{H}_C$, and describe it using the density operator formalism to obtain $\hat{\rho}(t) = |\Psi(t)\rangle\langle\Psi(t)|$. Sequentially, we arbitrarily trace out the degree of freedom C , resulting in the reduced density matrix $\hat{\rho}_B(t) = \text{Tr}_C[\hat{\rho}(t)]$. We then compute the von Neumann entropy $S_B(t) = -\text{Tr}[\hat{\rho}_B(t) \log \hat{\rho}_B(t)]$ to quantify the amount of mixedness. A zero entropy indicates that the reduced density matrix $\hat{\rho}_B(t)$ is pure, and hence the state $|\psi_{BC}\rangle$ is separable. Conversely, a nonzero entropy implies that $\hat{\rho}_B(t)$ is a mixed state, signaling that the state $|\Psi(t)\rangle$ is entangled. In this scenario, the mixedness is proportional to the entanglement, as it reflects the uncertainty in the individual subsystem.

[15]. A more rigorous analysis was conducted by Phoenix and Knight in 1988 [16], with the term “entanglement” being used for the first time in 1991 [17] by the same authors. Since then, due to its relevance in quantum computing applications, the nonseparability of the state in the JC model has been extensively investigated [84–89]. To compute entanglement in the context of the JC model, we begin with the evolved state described in Eq. (15) and its corresponding probability amplitudes, Eq. (16). By definition, the density matrix of the system is $\hat{\rho}(t) = |\Psi(t)\rangle\langle\Psi(t)|$. Tracing out the cavity degree of freedom we obtain the reduced density operator for the atom

$$\hat{\rho}_A(t) = \text{Tr}_F[\hat{\rho}(t)] = \sum_{n=0}^{\infty} \langle n | \hat{\rho}(t) | n \rangle, \quad (22)$$

matrixially represented by

$$\hat{\rho}_A(t) = \begin{pmatrix} P_e(t) & \xi(t) \\ \xi^*(t) & P_g(t) \end{pmatrix}. \quad (23)$$

The coherence term is given by $\xi(t) = \sum_{n=0}^{\infty} C_{e,n}^*(t) C_{g,n}(t)$ and the diagonal elements are the atomic populations, Eq. (17). The instantaneous eigenvalues can be computed from the characteristic equation $\det[\hat{\rho}_A(t) - \mu_i(t)\hat{I}] = 0$, and are given by

$$\mu_{\pm}(t) = \frac{1}{2} \left(1 \pm \sqrt{W^2(t) + 4|\xi(t)|^2} \right), \quad (24)$$

can be used to compute the von Neumann entropy, Eq. (21). The behavior of the entanglement in this situation is presented in Fig. 3, alongside the population inversion. We observe that the system is nearly separable approximately at the center of

the collapse region, while exhibiting relatively high entanglement during the revival phase. In general, the separability of the system can be understood by expressing the joint atom-field state in the eigenbasis that diagonalizes $\hat{\rho}_A(t)$:

$$|\Psi(t)\rangle = \vartheta_+(t)|\psi_A^+(t), \psi_F^+(t)\rangle + \vartheta_-(t)|\psi_A^-(t), \psi_F^-(t)\rangle, \quad (25)$$

where $|\vartheta_{\pm}(t)|^2 = \mu_{\pm}(t)$, $\{|\psi_A^i(t)\rangle, i = +, -\}$ and $\{|\psi_F^i(t)\rangle, i = +, -\}$, represent time-dependent eigenbases. For example, the entanglement is nearly zero when $\mu_+(t) \gg \mu_-(t)$, which happens in the collapse region [80]. As a consequence, the atom-field state can be written as $|\Psi(t)\rangle \approx |\psi_A^+(t), \psi_F^+(t)\rangle$. We emphasize that Eq. (25) expresses the Schmidt decomposition of the JC model.

III. TIME-DEPENDENT COUPLING DYNAMICS

As mentioned in Sec. I, the Hamiltonian of the TDJC model is a modified version of the JC Hamiltonian, Eq. (1), with explicit time dependence in parameters that are usually fixed. This approach was first implemented by Schlicher [41], who considered a sinusoidal coupling parameter and studied transparency effects. Solving the TDJC model off-resonance often requires numerical methods, with analytical solutions being the exception unless additional approximations are applied [43, 44, 46, 47]. A recent and compelling development in this area is the utilization of the symmetry properties of the JC Hamiltonian to analyze the system [40].

In this work, we are interested in how time-dependent coupling parameters affect the on-resonance dynamics of the JC model. Other works that adopt a similar approach can be found in Refs. [41, 42, 48, 90, 91].

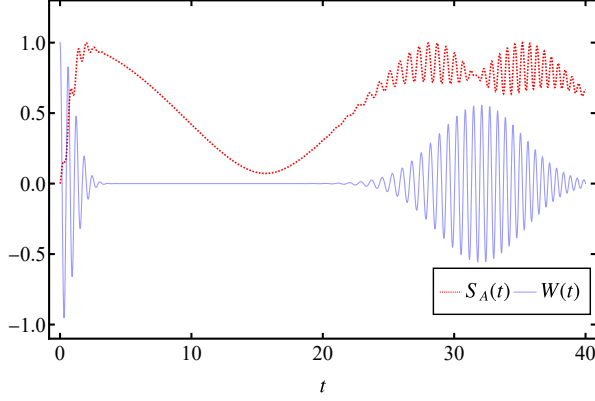


FIG. 3. The population inversion (solid blue line) and von Neumann entropy (dotted red line) as a function of the dimensionless time, when considering the initial state $|\Psi(0)\rangle = |e, \alpha\rangle$, an average photon number of $\langle n \rangle = 25$, and a constant coupling parameter $\lambda_0 = 1$.

The change $\lambda \rightarrow \lambda(t)$ makes the Hamiltonian, Eq. (4), explicitly time-dependent, while it still commutes with itself at different instants. As a result, the time evolution operator is described as

$$\hat{U}(t) = \exp \left[-i \int_0^t \hat{V}(t') dt' \right], \quad (26)$$

instead of the expression in Eq. (7) [69]. Here, we introduce the coupling-area, defined as [24, 41]

$$A(t) = \int_0^t \lambda(t') dt'. \quad (27)$$

The algebraic procedures realized in Sec. II remain the same, with the change $\lambda t \rightarrow A(t)$ in the final result [54]. Thus

$$\begin{aligned} \hat{U}(t) = & \cos \left[A(t) \sqrt{\hat{a}^\dagger \hat{a} + 1} \right] |e\rangle \langle e| \\ & + \cos \left[A(t) \sqrt{\hat{a}^\dagger \hat{a}} \right] |g\rangle \langle g| \\ & - i \frac{\sin \left[A(t) \sqrt{\hat{a}^\dagger \hat{a} + 1} \right]}{\sqrt{\hat{a}^\dagger \hat{a} + 1}} \hat{a} |e\rangle \langle g| \\ & - i \frac{\sin \left[A(t) \sqrt{\hat{a}^\dagger \hat{a}} \right]}{\sqrt{\hat{a}^\dagger \hat{a}}} \hat{a}^\dagger |g\rangle \langle e|. \end{aligned} \quad (28)$$

Fixing the initial state as $|\Psi(0)\rangle = |e, \alpha\rangle$ and employing the time-evolution operator, Eq. (28), the probability amplitudes can be generalized for an arbitrary time-dependent coupling as follows

$$\begin{aligned} C_{e,n}(t) &= C_n \cos \left[A(t) \sqrt{n+1} \right], \\ C_{g,n}(t) &= -i C_{n-1} \sin \left[A(t) \sqrt{n} \right], \end{aligned} \quad (29)$$

where C_n is governed by Eq. (14). The same approach as before can be applied to the population inversion, yielding

$$W(t) = \sum_{n=0}^{\infty} P_n \cos \left[2A(t) \sqrt{n+1} \right]. \quad (30)$$

Here $P_n = |C_n|^2$ is the photon number probability distribution of the initial field state. The reason the JC model retains much of its structure in this generalization is that it preserves its block structure, even with the time-dependent coupling parameter [24]. This occurs because the excitation number operator, Eq. (2), remains a constant of motion, which can be verified by computing its expectation value.

In the following subsections, we will compute the population inversion and entanglement for two distinct time dependencies in the coupling parameter. The procedure is straightforward: (i) we first calculate the coupling area, $A(t)$; (ii) using Eq. (29), we compute the state vector; (iii) from the state vector, we obtain the density operator; (iv) from the density operator, we calculate the entropy; and (v) using Eq. (30), we compute the population inversion. Additionally, we note that our presentation of the modulation forms differs from that in the original references, as we express them in terms of two constant parameters, λ_0 and ζ , both having the same dimension as $\lambda(t)$.

A. Linear

Joshi and Lawande [48] considered the linear coupling modulation, given by

$$\lambda(t) = \lambda_0 \zeta_1 t, \quad (31)$$

where λ_0 and ζ_1 are control parameters that determine whether the change in the coupling is either sudden or adiabatic. According to Ref. [24], this modulation can be used to represent the scenario of a well-localized atom in a spatially varying mode. The authors observed that, for an initial coherent field state, this time-dependent coupling alters the revival time. More recently, Hu and Tan [92] studied a double JC model with linear modulation, focusing on the disappearance of entanglement between the two atoms. They suggested that a linear coupling parameter could be realized in cavity quantum electrodynamics by controlling the intensity of an external electric field.

For an initial state $|\Psi(0)\rangle = |e, \alpha\rangle$, the population inversion resulting from the linear coupling is

$$W(t) = \sum_{n=0}^{\infty} P_n \cos \left(\sqrt{n+1} \lambda_0 \zeta_1 t^2 \right). \quad (32)$$

As shown in Fig. 4, the quadratic time dependence in the arguments of the cosine functions in Eq. (32) leads to denser Rabi oscillations than in the standard JC model. In addition, we observe in Fig. 4(a) (Fig. 4(b)) a sudden (adiabatic) change in the coupling, corresponding to larger (smaller) values of ζ_1 , increases (decreases) the Rabi frequencies, resulting in a denser (less dense) atomic inversion curve and a shorter (longer) first revival time, now given by $t_r = 2\sqrt{\pi \langle \hat{n} \rangle^{1/2} / \zeta_1 \lambda_0}$ [48]. Besides, following the shift in the revival time, the behavior of the von Neumann entropy is also affected. In the sudden change case, the minimum entanglement is achieved earlier than in the usual scenario, whereas under adiabatic change, it occurs later.

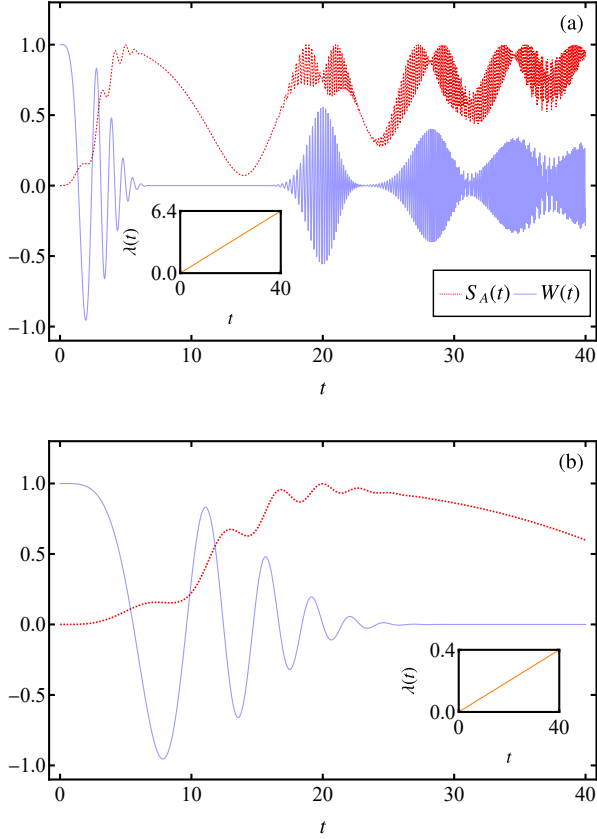


FIG. 4. The population inversion (solid blue line) and von Neumann entropy (dotted red line) as a function of dimensionless time, when considering the initial state $|\Psi(0)\rangle = |e, \alpha\rangle$, an average photon number of $\langle n \rangle = 25$, $\lambda_0 = 1$ and the linear modulation. In (a), we depict the sudden change in the coupling, with $\zeta_1 = 0.16$, while in (b) we represent the adiabatic change, $\zeta_1 = 0.01$. As an inset in both plots, we present the behavior of the time-dependent coupling. We observe a change in the entanglement dynamics, with its minimum and maximum occurring at different times compared to the constant coupling scenario.

B. Hyperbolic Secant

Dasgupta [44] suggested the coupling modulation

$$\lambda(t) = \lambda_0 \operatorname{sech}(\zeta_2 t), \quad (33)$$

This type of coupling, can be used to simulate transient effects in the cavity, allowing the interaction to be switched on and off depending on the choice of the initial time. The population inversion in this scenario is given by

$$W(t) = \sum_{n=0}^{\infty} P_n \cos \left\{ \frac{2\lambda_0 \sqrt{n+1}}{\zeta_2} \tan^{-1} [\sinh(\zeta_2 t)] \right\}. \quad (34)$$

In Fig. 5, we observe how this coupling, which decays to zero, can lead to different asymptotic values for both population inversion and entanglement. In Fig. 5(a), we set $\zeta_2 = 0.3$ (faster decay of coupling), causing the dynamics to halt before

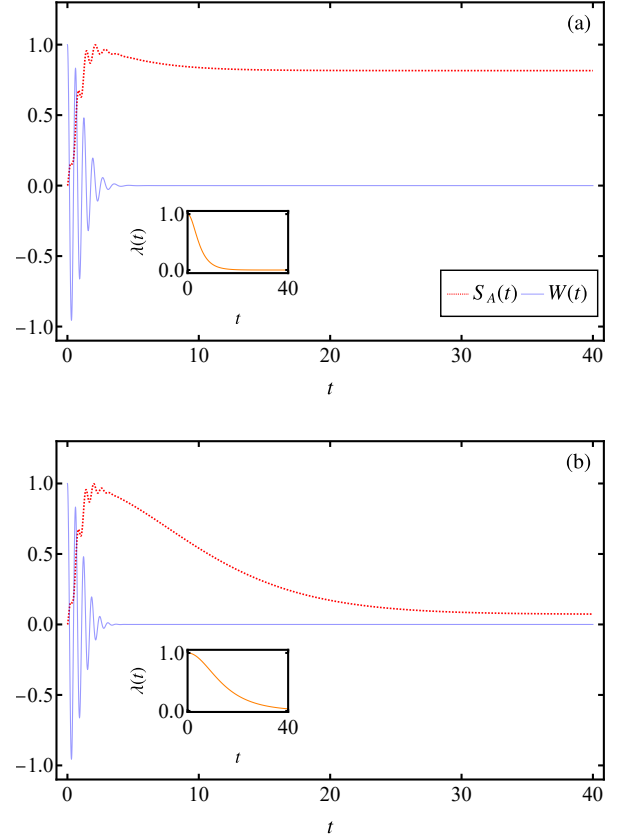


FIG. 5. The population inversion (solid blue line) and von Neumann entropy (dotted red line) as a function of dimensionless time, when considering the initial state $|\Psi(0)\rangle = |e, \alpha\rangle$, an average photon number of $\langle n \rangle = 25$, $\lambda_0 = 1$ and the hyperbolic secant modulation. In (a), we present a faster decay in the coupling, with $\zeta_2 = 0.3$, while in (b) we represent a slower stabilization, $\zeta_2 = 0.1$. As an inset in both plots, we present the behavior of the time-dependent coupling. We observe an asymptotic value for both the population inversion and the entanglement.

reaching the revival time. In contrast, in Fig. 5(b), we adopt a slower decay for the coupling. In both cases, the dynamics cease after the collapse, causing the asymptotic value of $W(t)$ to be 0. However, for another combination of parameters, it would be possible to obtain different asymptotic values. Furthermore, another important aspect is that, even though the asymptotic value of the population inversion is the same in both cases, the von Neumann entropy value is significantly different. The coherence terms of the density matrix, which do not affect the atomic probabilities, are influenced by the different atom-field decoupling times, and this is reflected in the entanglement behavior.

This concludes the tutorial part of this work. In the following section, we examine aspects of the atomic dynamics considering a sinusoidally varying coupling parameter and assuming a thermal initial state for the cavity field.

IV. ATOMIC MOTION

As mentioned in the previous section, Schlicher was the first to introduce a time-dependent coupling parameter. In that context, he employed a sinusoidal modulation to account for the motion of the atom along the standing-wave [41]. Since then, this type of time dependence has been extensively studied: Bartzis investigated squeezing in the cavity degree of freedom [90], Wilkens and Meystre extended the approach to maser systems [93], and Fang computed the von Neumann entropy and the Husimi function [42], considering an initial coherent state of the cavity. Other works regarding atomic motion in the model can be found in Refs. [94–98]. In this case, we adopt a semiclassical approach, in which the atomic motion is treated classically—an approximation justified when the atom’s kinetic energy significantly exceeds the interaction energy of the JC model [24].

We next address the situation of having the field initially in a thermal state. The study of the JC model considering such a state [71] was first conducted by Cummings [5] and later explored in greater depth by Knight and Radmore [99]. This corresponds to a partially cooled cavity [14], which is a more realistic scenario given the difficulty of cooling a cavity very close to $T = 0$ K [9]. Unlike the generally well-defined collapses and revivals observed in the case of an initial coherent state, for a thermal state, the population inversion exhibits an erratic time evolution due to large photon number fluctuations. Later, Arancibia-Bulnes et al., [57] and Azuma [56] investigated the evolution of the Bloch vector in the JC model with an initial thermal field, the latter concluding that the “thermal JC model” could serve as a future source of entanglement. Additional studies on the model with an initial thermal state, but without taking into account the atomic motion, can be found in Refs. [14, 15, 53, 74, 100–104].

The combination of atomic motion with an initial thermal field state has been explored less frequently: Yan studied two successive atoms passing a cavity and observed entanglement sudden death [54], while Joshi investigated the dependence of population inversion on detuning, for different initial states of the atom, with a focus on how the TLS follows the field adiabatically [55].

In this work, we first analyze the time evolution of the population inversion, examining the effects of both the periodicity of the sinusoidal coupling parameter and the significant uncertainty associated with the thermal state. The coupling parameter is modeled as

$$\lambda(t) = \lambda_0 \sin\left(\frac{p\pi vt}{L}\right), \quad (35)$$

where p represents the number of half-wave lengths of the field mode, v is the atomic velocity and L is the cavity length. Henceforth, we assume that the velocity is $v = \zeta_3 L/\pi$. In this context, the coupling area, Eq. (27), is

$$A(t) = \frac{\lambda_0 [1 - \cos(p\zeta_3 t)]}{p\zeta_3}. \quad (36)$$

Thus, having λt replaced by the periodic function $A(t)$ in the time evolution operator, we expect the system to exhibit pe-

riodic behavior, as shown in Ref. [42]. This may have a significant impact on the time evolution of the atomic population inversion, for instance, as we are going to show below. We remark that the parameters p and ζ_3 affect the system’s dynamics in the same way, even though they represent different quantities.

Given that the initial field state of the system is mixed, we must employ the density operator formalism. We assume the TLS initially in the excited state, $\hat{\rho}_A(0) = |e\rangle\langle e|$, and write the initial thermal field state as [79]

$$\hat{\rho}_F(0) = \sum_{n=0}^{\infty} P_n |n\rangle\langle n|, \quad (37)$$

where

$$P_n = \frac{\langle n \rangle^n}{(1 + \langle n \rangle)^{n+1}}, \quad (38)$$

is the Bose-Einstein distribution. The average photon number $\langle n \rangle = [\exp(\nu/k_B T) - 1]^{-1}$ can be expressed in terms of the frequency ν and the effective temperature T , where k_B denotes the Boltzmann constant. The joint atom-field state evolves according to

$$\hat{\rho}(t) = \hat{U}(t)\hat{\rho}(0)\hat{U}^\dagger(t), \quad (39)$$

where $\hat{U}(t)$ is the time evolution operator given in Eq. (28). Additionally, we consider an initially separable state of the system $\hat{\rho}(0) = \hat{\rho}_A(0) \otimes \hat{\rho}_F(0)$. Following Eqs. (39), (22) and (36), considering the initial excited atomic state, we obtain the evolved atomic density matrix [62, 84]

$$\begin{aligned} \hat{\rho}_A(t) = \sum_{n=0}^{\infty} P_n \{ & \cos^2[A(t)\sqrt{n+1}] |e\rangle\langle e| \\ & + \sin^2[A(t)\sqrt{n+1}] |g\rangle\langle g| \}. \end{aligned} \quad (40)$$

Therefore, the population inversion in this scenario is explicitly given by

$$W(t) = \sum_{n=0}^{\infty} P_n \cos\left\{ \frac{2\lambda_0 \sqrt{n+1}}{p\zeta_3} [1 - \cos(p\zeta_3 t)] \right\}, \quad (41)$$

where we have employed Eqs. (35) and (27), and P_n corresponds to the Bose-Einstein distribution, Eq. (38). Recall that the parameter ζ_3 is related to the atomic velocity v through $v = \zeta_3 L/\pi$. The time evolution of the population inversion is presented in Fig. 6. We observe that, rather than the erratic behavior associated with the thermal field state, the system exhibits periodicity, with a period that depends on the parameters p and ζ_3 . Additionally, secondary oscillations arise due to inflections in the coupling parameter, and if we compare the results with Ref. [42] for an initial coherent state, we note that the thermal state gives rise to RO with smaller amplitude, as expected when considering the constant coupling scenario [99].

In Fig. 7 we illustrate how the population inversion depends on relevant parameters of the system. In Fig. 7(a) we

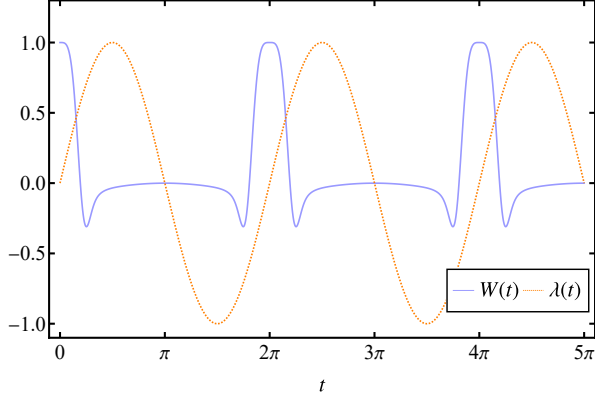


FIG. 6. The population inversion (solid blue line) and the coupling parameter (dotted orange line) as a function of dimensionless time, when considering the initial state excited state of the TLS and thermal state of the cavity, an average photon number of $\langle n \rangle = 25$, $\lambda_0 = 1$, $\zeta_3 = 1$, $p = 1$ and the velocity $v = \zeta_3 L/\pi$. As a consequence of the sinusoidal coupling, we observe a periodic evolution for the population inversion, even considering a strong initial thermal cavity field state.

have plotted $W(t)$ as a function of the initial average photon number, $\langle n \rangle$, and the dimensionless time. Although the period does not depend on $\langle n \rangle$, the concavity between adjacent two main peaks becomes wider as $\langle n \rangle$ increases, while its amplitude decreases. This occurs because a smaller $\langle n \rangle$ sharpens the probability distribution, which is reflected in the atomic inversion. Similarly, as shown in Fig. 7(b), while the period of the main oscillations is independent of the amplitude λ_0 , we clearly see the emergence of the secondary oscillations due to the inflections in $\lambda(t)$, which become more pronounced as λ_0 increases.

A. Bloch vector

If the global state of the system is mixed, the von Neumann entropy is no longer a suitable measure of entanglement [51, 62]. Considerable attention has been given to entanglement measures in this context [53, 84, 104], such as the concurrence in a system of two moving two-level atoms [54]. Alternatively, we focus here on the Bloch vector [105], which contains comprehensive information about the quantum state, including its purity and the degree of atom-field alignment. The Bloch vector $\mathbf{R}(t)$ is a convenient geometrical representation of the quantum states of two-level systems. It is such that $|\mathbf{R}(t)| \leq 1$ and can be associated with points in a unit sphere, known as *Bloch sphere*. While pure quantum states lie on the sphere's surface, $|\mathbf{R}(t)| = 1$, for mixed states $|\mathbf{R}(t)| < 1$. As any 2×2 matrix can be expressed as a linear combination of the Pauli matrices and the identity matrix $\mathbf{1}_2$, the reduced atomic density matrix can be parametrized as

$$\hat{\rho}_A(t) = \frac{1}{2}[\mathbf{1}_2 + \hat{\sigma} \cdot \mathbf{R}(t)]. \quad (42)$$

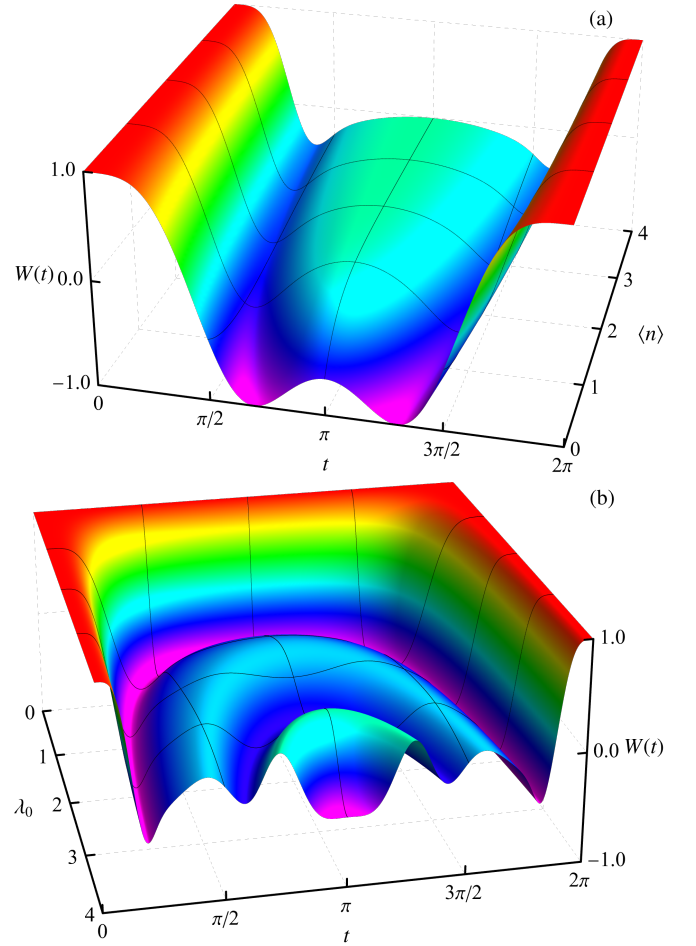


FIG. 7. In (a), we present a surface plot of the population inversion as a function of dimensionless time and the average number of photons, $\langle n \rangle$, with $\lambda_0 = 1$ fixed. An increase in $\langle n \rangle$ reduces the amplitude while enlarging the small concavity at the bottom. In (b), we present a surface plot of the population inversion as a function of dimensionless time and the parameter λ_0 , with $\langle n \rangle = 4$ fixed. An increase in λ_0 alters the oscillation shape. In both plots, we set $p = \zeta_3 = 1$, and $v = \zeta_3 L/\pi$.

Expressing the Bloch vector in terms of its components as

$$\mathbf{R}(t) = [R_x(t), R_y(t), R_z(t)], \quad (43)$$

we obtain

$$\begin{aligned} R_x(t) &= \langle \hat{\sigma}_x \rangle = \rho_A^{eg}(t) + \rho_A^{ge}(t), \\ R_y(t) &= i[\rho_A^{eg}(t) - \rho_A^{ge}(t)], \\ R_z(t) &= W(t) = \rho_A^{ee}(t) - \rho_A^{gg}(t), \end{aligned} \quad (44)$$

where ρ_A^{ij} represents the elements of $\hat{\rho}_A(t)$, with $i = e, g$. Interpretation-wise, the component $R_x(t)$ corresponds to the expectation value of the Pauli matrix in the x -direction, also known as the dipole operator, which quantifies the atom's alignment with the field [24]. It can be expressed by $\hat{\sigma}_x = \hat{\sigma}_+ + \hat{\sigma}_-$. Moreover, $R_z(t)$ represents the population inversion, while $R(t) = |\mathbf{R}(t)|$ serves as a measure of atomic purity [105].

It follows that $R(t)$ is inversely related to the von Neumann entropy, as the latter quantifies the mixedness of the atomic subsystem. We choose to focus on the Bloch vector – its motion, components, and modulus – for comparison with the results mentioned in the next paragraph.

The dynamics of the Bloch vector in the context of the JC model was first studied by Gea-Banacloche in 1992 [105], considering an initial coherent state in the cavity. As mentioned earlier, this analysis was later extended considering to the case of an initial thermal state, revealing erratic Bloch vector dynamics [56, 57]. In a subsequent study, Azuma and Ban demonstrated that this behavior exhibits a quasiperiodic structure [58]. Joshi and Xiao studied the simultaneous effects of atomic motion with an initial thermal state, considering detuning and the adiabatic approximation, and focusing on transparency effects [55]. Here, we explore the influence of atomic motion on the evolution of the Bloch vector, considering the cavity initially in a thermal state.

To analyze the dynamics of the Bloch vector in the xz plane, we modify the initial TLS state to an eigenvector of $\hat{\sigma}_x$, namely $|\psi_A(0)\rangle = 1/\sqrt{2}(|e\rangle + |g\rangle)$. In the density operator formalism, the initial state of the system is, then,

$$\hat{\rho}(0) = \left[\frac{1}{2} (|e\rangle\langle e| + |e\rangle\langle g| + |g\rangle\langle g| + |g\rangle\langle e|) \right] \otimes \hat{\rho}^F(0), \quad (45)$$

where $\hat{\rho}^F(0)$ is described by Eq. (37). This contrasts with the usual choice for the initial state, $\hat{\rho}_A(0) = |e\rangle\langle e|$, which yields a diagonal atomic density matrix without coherence terms, restricting the Bloch vector to the z -axis, as seen in Eq. (40). Additionally, this change facilitates comparison with previous results. Employing Eqs. (22), (28) and (39), and considering the initial state in Eq. (45), we obtain the evolved atomic density matrix

$$\begin{aligned} \hat{\rho}_A(t) = & \frac{1}{2} \sum_{n=0}^{\infty} P_n \left\{ \cos^2 [A(t) \sqrt{n+1}] + \sin^2 [A(t) \sqrt{n}] \right\} |e\rangle\langle e| \\ & + \frac{1}{2} \sum_{n=0}^{\infty} P_n \cos [A(t) \sqrt{n+1}] \cos [A(t) \sqrt{n}] |e\rangle\langle g| \\ & + \frac{1}{2} \sum_{n=0}^{\infty} P_n \cos [A(t) \sqrt{n}] \cos [A(t) \sqrt{n+1}] |g\rangle\langle e| \\ & + \frac{1}{2} \sum_{n=0}^{\infty} P_n \left\{ \cos^2 [A(t) \sqrt{n}] + \sin^2 [A(t) \sqrt{n+1}] \right\} |g\rangle\langle g|. \end{aligned} \quad (46)$$

From this result, we can calculate the components of the Bloch vector, according to Eq. (44),

$$\begin{aligned} R_x(t) &= \sum_{n=0}^{\infty} P_n \cos [A(t) \sqrt{n}] \cos [A(t) \sqrt{n+1}], \\ R_y(t) &= 0, \\ R_z(t) &= \sum_{n=0}^{\infty} P_n \left\{ \cos^2 [A(t) \sqrt{n+1}] + \sin^2 [A(t) \sqrt{n}] \right\} - 1. \end{aligned} \quad (47)$$

In Fig. 8, we present the motion of the Bloch vector for both constant and sinusoidal coupling scenarios. In the constant coupling case, shown in Fig. 8(a) and (e), we set $\lambda = 1$. For the sinusoidal coupling case, depicted in the other panels of Fig. 8, we fix the parameters as $\lambda_0 = 1$ and $v = \zeta_3 L/\pi$. In panels (b), (c), (f) and (g), we set $p = 1$, while in panels (d), and (h), we set $p = 2$. In (b) and (g), we employ $\zeta_3 = 0.25$, while in the other panels, we fix $\zeta_3 = 1$. At the outset, we choose a low average photon number, $\langle n \rangle = 0.5$, corresponding to a low temperature, for all scenarios. Comparing panels (a) and with (b), (c) and (d), we observe that the sinusoidal coupling introduces periodicity into the Bloch vector's motion, replacing the disordered behavior. In contrast, for a smaller ζ_3 , as shown in (b), the behavior partially resembles that of the time-independent coupling case, exhibiting reduced-amplitude oscillations within each period. This suggests that for lower values of the parameter ζ_3 , an intermediate regime emerges in which vestiges of the aperiodic evolution persist. In Figs. 8(f), (g) and (h), which show the components and absolute value of the Bloch vector, we again observe the periodicity inherited from the modulated coupling, as compared to Fig. 8(e). Furthermore, as shown in the panels where atomic motion is considered, an increase in p and ζ_3 results in a higher frequency of the oscillations, while the amplitudes of the oscillations in $R_x(t)$ and $R(t)$ decrease. As a result, the atom tends to be more aligned with the field, leading to a higher time-averaged purity of the atomic state, whereas $R_z(t)$ oscillates with approximately the same amplitude. In all examples with atomic motion, we begin with $R(0) = R_x(0) = 1$ and $R_z(0) = 0$, meaning that initially, the atomic subsystem is pure, the atomic transition is aligned with the field and the excited and ground populations are equal. This behavior is a direct consequence of the trigonometric dependence of the coupling area $A(t)$, as discussed previously, which can also be interpreted in terms of Bloch vector rotations for the chosen velocity, as predicted by Joshi and Xiao [55].

A question that arises is how increasing the mean photon number of the initial thermal state affects the Bloch vector dynamics. On the one hand, sinusoidal modulation of the coupling induces a periodic evolution of the Bloch vector; on the other, stronger thermal fluctuations are expected to produce a more disordered evolution. For instance, considering a larger initial average photon number, we expect a reduction in the time-averaged purity due to the increase of thermal fluctuations. Nevertheless, increasing $\langle n \rangle$ gives rise to another effect, a kind of *atomic population trapping*. This is clearly shown in Fig. 9, where we plot the Bloch vector trajectory for two different initial mean photon numbers, $\langle n \rangle = 5$ and $\langle n \rangle = 25$. Thus, increasing the thermal noise does not significantly enhance the disorder in the evolution, which remains dominated by the periodic forcing, but instead tends to freeze the atomic population. A similar effect occurs in the constant-coupling case, as discussed in Ref. [57]. We remark that this kind trapping differs in nature from the population trapping found in the JC model with an initial coherent state [106, 107]. In the present case, the trapping arises from the cancellation of photon emission (absorption) by the upper (lower) atomic state [57], whereas in the coherent state case it is a phase-dependent

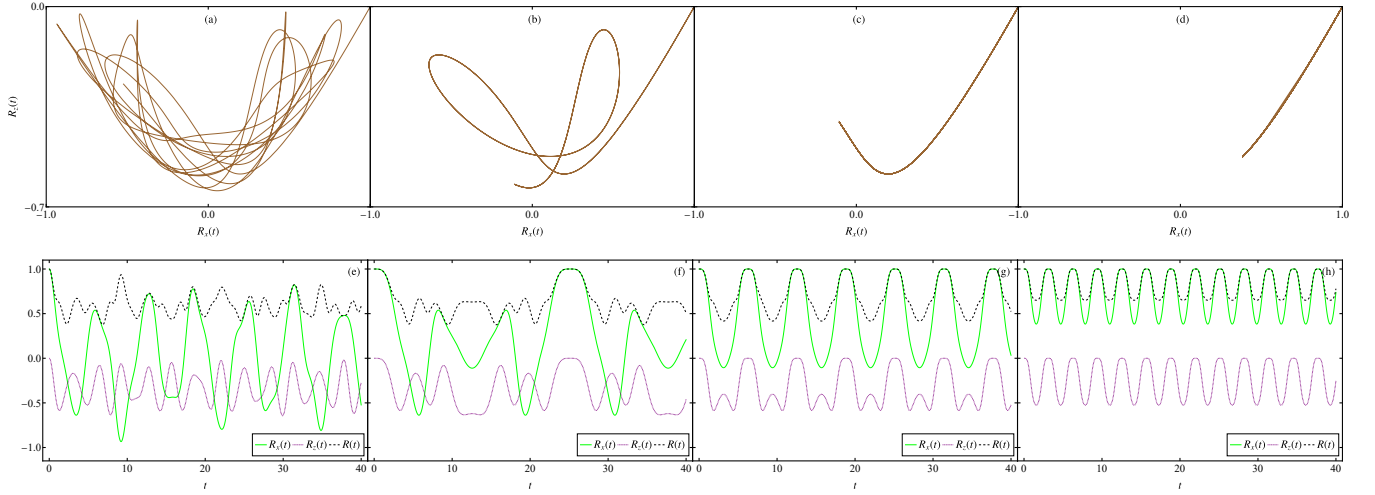


FIG. 8. Trajectories and time-evolution of the Bloch vector. In panels (a) and (e), atomic motion is not considered, and we set the parameter $\lambda = 1$. Conversely, in the remaining panels, atomic motion is included, with parameters $\lambda_0 = 1$, $v = \zeta_3 \pi / L$ and considered a time interval $0 < t < 40$. In panels (b), (c), (f) and (g), we set $p = 1$, whereas in panels (d) and (h), we use $p = 2$. In (b) and (f), we employ $\zeta_3 = 0.25$, while in the other panels, we fix $\zeta_3 = 1$. In all cases, the initial average photon number is $\langle n \rangle = 0.5$. In panels (a), (b), (c) and (d), we present a parameter plot of the $R_x(t)$ and $R_z(t)$ components as a function of time. We observe that atomic motion dominates the disordered behavior of the Bloch vector. Panels (e), (f), (g) and (h) depict the time evolution of $R_x(t)$ (solid green line), $R_z(t)$ (dotted purple line), and $R(t)$ (dashed black line). The periodicity once again reveals the presence of sinusoidal coupling. Additionally, an increase in p diminishes the amplitude of $R_x(t)$ and $R(t)$.

phenomenon [106, 107].

Several other modulations can be found in the literature, which the reader may eventually find useful. For instance, an alternative to simulate transient effects in the cavity, the exponential dependence has been considered by Prants [43]. In Ref. [46], various distinct coupling pulses, such as square, Gaussian, and Lorentzian waves, were used to analyze the perspective of photon filters. Besides, the sinusoidal time dependence has its generalizations, including cases of accelerating atoms [97], where the argument of the trigonometric function

is quadratic in time, or the alignment of the atom's dipole moment [98], where the sine function appears squared. An explicit approach to controlling the population inversion via the time-dependent coupling parameter is detailed in Ref. [91].

V. CONCLUSIONS

In the context of the 100-year anniversary of quantum mechanics, the Jaynes-Cummings model stands as a cornerstone for understanding light-matter interaction. More than half a century after its introduction, its exact solvability and conceptual clarity continue to inspire both theoretical developments and experimental implementations at the frontiers of quantum science and technology. Building on this legacy, we have investigated the resonant time-dependent Jaynes-Cummings model, where the modulation of the atom-field coupling parameter may simulate physical phenomena such as transient behavior and atomic motion. We presented a pedagogical derivation of a solution of the time-dependent Jaynes-Cummings model valid for a wide range of initial conditions, assuming a time-dependent atom-field coupling. The first type of modulation considered was a linear ramp, associated with variations in the cavity mode. We observed that the behavior of entropy and population inversion was significantly affected by the control parameter ζ_1 , the slope of the ramp, which can delay or advance the evolution of the Rabi oscillations. The second type of coupling modulation, given by a hyperbolic secant function, accounted for transient effects in the cavity, such as switching on and off. Our results indicated that, by simulating the gradual turning off of the cavity, asymptotic

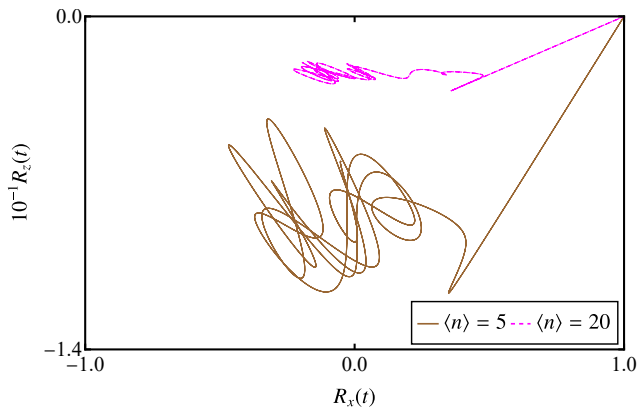


FIG. 9. Bloch vector trajectories for larger initial average thermal photon numbers considering atomic motion with (i) $\langle n \rangle = 5$ (solid brown line) and (ii) $\langle n \rangle = 20$ (dashed magenta line). We set $\lambda_0 = 1$, $p = 1$ and $\zeta_3 = 0.1$ and considered a time interval $0 < t < 100$.

values of the atom-field entanglement can be reached, depending on the control parameter ζ_2 , which sets the time scale of the atom-field coupling decay. Entanglement plays a central role in quantum information processing, and these modulations offer a way of controlling it. Next, we examined another physically relevant scenario in which an atom moves inside a cavity that is not completely cooled, analyzing the resulting behavior of the population inversion. As a consequence of the trigonometric coupling, the Rabi oscillations became periodic, in contrast to the constant-coupling scenario. We also investigated how the parameters $\langle n \rangle$ and λ_0 affect the population inversion. The average initial photon number $\langle n \rangle$ influences the amplitude of the oscillations, also widening the concave region between neighboring main peaks, while λ_0 introduces secondary oscillations due to the inflection in the coupling parameter.

Finally, we analyzed the influence of atomic motion on the dynamics of the Bloch vector, a quantity that provides an accurate characterization of the system, considering the atom initially prepared in a superposition of ground and excited states (an eigenvector of $\hat{\sigma}_x$). Our analysis revealed a number of interesting aspects of the system. Unlike the disordered dynamics in the constant-coupling scenario, the periodically varying atom-field coupling parameter leads to a periodic evolution of the Bloch vector trajectories, dominating over thermal fluctuations. However, for sufficiently small values of the control parameter ζ_3 , proportional to the frequency of the coupling modulation, we observe longer-period oscillations, resembling the dynamics of the constant-coupling case. On the other hand, increasing either the number of half-wavelengths in the field structure, p , or the parameter ζ_3 , which is proportional to the atomic velocity, results in a larger time-averaged purity of the atomic subsystem. Our results also reveal an interesting underlying competition in the dynamics: increasing the average thermal photon number, instead of introduc-

ing further disorder into the Bloch vector trajectories, induces a type of population trapping effect. As quantum mechanics reaches its centenary, the Jaynes–Cummings model, over 60 years old yet distinguished by its blend of simplicity and depth, continues to thrive, advancing our understanding of light–matter interaction as well as offering useful guidance for applications in quantum technologies.

ACKNOWLEDGMENTS

We thank Dr. Alison A. Silva for helpful discussions. This work was financially supported by the Coordenação de Aperfeiçoamento de Pessoal de Nível Superior (CAPES, Finance Code 001), Conselho Nacional de Desenvolvimento Científico e Tecnológico (CNPq), Instituto Nacional de Ciência e Tecnologia de Informação Quântica (INCT-IQ), Brazil, and the Air Force Office of Scientific Research (AFOSR), USA. DC would like to acknowledge financial support from Instituto Serrapilheira, and the Pró-Reitoria de Pesquisa e Inovação (PRPI) from the Universidade de São Paulo (USP) by financial support through the Programa de Estímulo à Supervisão de Pós-Doutorandos por Jovens Pesquisadores. F.M.A. acknowledges the CNPq Grant No 313124/2023-0, and A.V.-B. acknowledges the AFOSR award No FA9550-24-1-0009.

Author Contributions The work is partly the result of T.T.T.’s PhD thesis under the supervision of F.M.A. and A.S.M.C.. The authors performed all calculations, figures, and graphs in partnership. T.T.T. and D.C. calculated the quantities in the dynamics. T.T.T. and A.V.-B. wrote the main manuscript text. All authors reviewed the manuscript.

Conflict of Interest The authors declare no competing interests.

Data Availability No datasets were generated or analyzed during the current study.

-
- [1] E. T. Jaynes and F. W. Cummings, *Proc. IEEE* **51**, 89 (1963).
 - [2] J. Larson, T. Mavrogordatos, S. Parkins, and A. Vidiella-Barranco, *J. Opt. Soc. Am. B* **41**, JCM1 (2024).
 - [3] D. De Bernardis, A. Mercurio, and S. De Liberato, *J. Opt. Soc. Am. B* **41**, C206 (2024).
 - [4] F. W. Cummings, *J. Phys. B* **46**, 220202 (2013).
 - [5] F. W. Cummings, *Phys. Rev.* **140**, A1051 (1965).
 - [6] P. Meystre, E. Geneux, A. Quattropiani, and A. Faist, *Il Nuovo Cimento B* **25**, 521 (1975).
 - [7] J. H. Eberly, N. B. Narozhny, and J. J. Sanchez-Mondragon, *Phys. Rev. Lett.* **44**, 1323 (1980).
 - [8] D. Meschede, H. Walther, and G. Müller, *Phys. Rev. Lett.* **54**, 551 (1985).
 - [9] G. Rempe, H. Walther, and N. Klein, *Phys. Rev. Lett.* **58**, 353 (1987).
 - [10] M. Brune, F. Schmidt-Kaler, A. Maali, J. Dreyer, E. Hagley, J. M. Raimond, and S. Haroche, *Phys. Rev. Lett.* **76**, 1800 (1996).
 - [11] J. R. Kukliński and J. L. Madajczyk, *Phys. Rev. A* **37**, 3175 (1988).
 - [12] M. Hillery, *Phys. Rev. A* **39**, 1556 (1989).
 - [13] M. Hillery, *Phys. Rev. A* **35**, 4186 (1987).
 - [14] S. M. Chumakov, M. Kozierowski, and J. J. Sanchez-Mondragon, *Phys. Rev. A* **48**, 4594 (1993).
 - [15] P. K. Aravind and J. O. Hirschfelder, *J. Phys. Chem.* **88**, 4788 (1984).
 - [16] S. J. D. Phoenix and P. L. Knight, *Ann. Phys.* **186**, 381 (1988).
 - [17] S. J. D. Phoenix and P. L. Knight, *Phys. Rev. A* **44**, 6023 (1991).
 - [18] G.-C. Guo and S.-B. Zheng, *Phys. Lett. A* **223**, 332 (1996).
 - [19] C. C. Gerry and R. Grobe, *Phys. Rev. A* **56**, 2390 (1997).
 - [20] C. A. Blockley, D. F. Walls, and H. Risken, *EuroPhys. Lett. (EPL)* **17**, 509 (1992).
 - [21] W. Vogel and R. L. de Matos Filho, *Phys. Rev. A* **52**, 4214 (1995).
 - [22] J. S. Pedernales, I. Lizuain, S. Felicetti, G. Romero, L. Lamata, and E. Solano, *Sci. Rep.* **5**, 15472 (2015), [arXiv:1505.00698](https://arxiv.org/abs/1505.00698).

- [23] A. Bermudez, M. A. Martin-Delgado, and E. Solano, *Phys. Rev. A* **76**, 041801 (2007).
- [24] J. Larson and T. Mavrogordatos, *The Jaynes–Cummings Model and Its Descendants* (IOP Publishing, Bristol, 2021).
- [25] N. Meher and S. Sivakumar, *Eur. Phys. J. Plus* **137**, 985 (2022).
- [26] W. K. Lai, V. Buek, and P. L. Knight, *Phys. Rev. A* **44**, 6043 (1991).
- [27] Y. Wu and X. Yang, *Phys. Rev. A* **56**, 2443 (1997).
- [28] R. H. Dicke, *Phys. Rev.* **93**, 99 (1954).
- [29] M. Tavis and F. W. Cummings, *Phys. Rev.* **170**, 379 (1968).
- [30] M. Chaichian, D. Ellinas, and P. Kulish, *Phys. Rev. Lett.* **65**, 980 (1990).
- [31] A. Dehghani, B. Mojaveri, S. Shirin, and S. A. Faseghandis, *Sci. Rep.* **6**, 38069 (2016).
- [32] G. M. Uhdre, D. Cius, and F. M. Andrade, *Phys. Rev. A* **105**, 013703 (2022).
- [33] V. Bužek and I. Jex, *Opt. Commun.* **78**, 425 (1990).
- [34] V. Bužek and I. Jex, *J. Mod. Opt.* **38**, 987 (1991).
- [35] I. A. Bocanegra-Garay, L. Hernández-Sánchez, I. Ramos-Prieto, F. Soto-Eguibar, and H. M. Moya-Cessa, *SciPost Phys.* **16**, 007 (2024).
- [36] A. Vidiella-Barranco, A. S. Magalhães de Castro, A. Sergi, J. A. Roversi, A. Messina, and A. Migliore, *Annalen der Physik* **n/a**, e00148.
- [37] R. R. Puri and G. S. Agarwal, *Phys. Rev. A* **33**, 3610 (1986).
- [38] S. M. Barnett and P. L. Knight, *Phys. Rev. A* **33**, 2444 (1986).
- [39] M. Scala, B. Militello, A. Messina, J. Piilo, and S. Maniscalco, *Phys. Rev. A* **75**, 013811 (2007).
- [40] A. S. M. de Castro, R. Grimaudo, D. Valenti, A. Migliore, H. Nakazato, and A. Messina, *Eur. Phys. J. Plus* **138**, 766 (2023).
- [41] R. R. Schlicher, *Opt. Commun.* **70**, 97 (1989).
- [42] M.-F. Fang, *Physica A Stat. Mech. Appl.* **259**, 193 (1998).
- [43] S. Prants and L. Yacoupova, *J. Mod. Opt.* **39**, 961 (1992).
- [44] A. Dasgupta, *J. Opt. B* **1**, 14 (1999).
- [45] A. Joshi, *J. Mod. Opt.* **42**, 2561 (1995).
- [46] J. Larson and S. Stenholm, *J. Mod. Opt.* **50**, 2705 (2003).
- [47] J. Keeling and V. Gurarie, *Phys. Rev. Lett.* **101**, 033001 (2008).
- [48] A. Joshi and S. V. Lawande, *Phys. Rev. A* **48**, 2276 (1993).
- [49] D. Maldonado-Mundo, P. Öhberg, B. W. Lovett, and E. Andersson, *Phys. Rev. A* **86**, 042107 (2012).
- [50] D. Dong and I. Petersen, *IET Control Theory Appl.* **4**, 2651 (2010).
- [51] M. A. Nielsen and I. L. Chuang, *Quantum Computation and Quantum Information: 10th Anniversary Edition* (Cambridge University Press, Cambridge, 2010).
- [52] L. Hernández-Sánchez, I. A. Bocanegra-Garay, I. Ramos-Prieto, F. Soto-Eguibar, and H. M. Moya-Cessa, *J. Opt. Soc. Am. B* **41**, C68 (2024).
- [53] S. Bose, I. Fuentes-Guridi, P. L. Knight, and V. Vedral, *Phys. Rev. Lett.* **87**, 050401 (2001).
- [54] X.-Q. Yan, *Chaos Solit. Fractals* **41**, 1645 (2009).
- [55] A. Joshi and M. Xiao, *J. Opt. Soc. Am. B* **21**, 1685 (2004).
- [56] H. Azuma, *Phys. Rev. A* **77**, 063820 (2008).
- [57] C. Arancibia-Bulnes, S. Chumakov, and J. Sánchez-Mondragón, *J. Mod. Opt.* **40**, 2071 (1993).
- [58] H. Azuma and M. Ban, *Phys. D: Nonlinear Phenom.* **280–281**, 22 (2014).
- [59] H. Azuma and M. Ban, *Physica D: Nonlinear Phenomena* **308**, 127 (2015).
- [60] J. Larson, *Phys. Scr.* **76**, 146 (2007).
- [61] M. O. Scully and M. S. Zubairy, *Quantum Optics* (Cambridge University Press, Cambridge, 1997).
- [62] C. Gerry and P. Knight, *Introductory Quantum Optics*, 2nd ed. (Cambridge University Press, Cambridge, 2004).
- [63] D. Braak, Q.-H. Chen, M. T. Batchelor, and E. Solano, *J. Phys. A* **49**, 300301 (2016).
- [64] A. B. Klimov and S. M. Chumakov, *A Group-Theoretical Approach to Quantum Optics* (Wiley-VCH, Weinheim, 2009).
- [65] R. R. S. Cantuba, *Int. Electron. J. Algebra* **35**, 32 (2024).
- [66] V. Kasper, G. Juzeliūnas, M. Lewenstein, F. Jendrzejewski, and E. Zohar, *New J. Phys.* **22**, 103027 (2020).
- [67] M. Bina, *Eur. Phys. J. Special Topics* **203**, 163 (2012).
- [68] R. Juárez-Amaro, A. Zúñiga-Segundo, and H. M. Moya-Cessa, *Appl. Math. Inf.* **9**, 299 (2015).
- [69] J. J. Sakurai and J. Napolitano, *Modern Quantum Mechanics*, 3rd ed. (Cambridge University Press, Cambridge, 2020).
- [70] M. Abramowitz and I. A. Stegun, eds., *Handbook of Mathematical Functions with Formulas, Graphs and Mathematical Tables*, 1st ed. (Dover, 1972).
- [71] R. J. Glauber, *Phys. Rev.* **131**, 2766 (1963).
- [72] C.-Y. Zhang and J. Jing, *Phys. Rev. A* **110**, 042421 (2024).
- [73] S. Haroche and J.-M. Raimond, *Exploring the Quantum* (Oxford University Press, 2006).
- [74] G. Arroyo-Correa and J. J. Sanchez-Mondragon, *Quant. Optics* **2**, 409 (1990).
- [75] R. Horodecki, P. Horodecki, M. Horodecki, and K. Horodecki, *Rev. Mod. Phys.* **81**, 865 (2009).
- [76] E. Schrödinger, *Naturwissenschaften* **23**, 807 (1935).
- [77] A. Einstein, B. Podolsky, and N. Rosen, *Phys. Rev.* **47**, 777 (1935).
- [78] J. S. Bell, *Physics Physique Fizika* **1**, 195 (1964).
- [79] J. von Neumann, *Gott. Nachr. Math. Phys. Klass.* (1927).
- [80] S. J. D. Phoenix and P. L. Knight, *J. Opt. Soc. Am. B* **7**, 116 (1990).
- [81] E. Schmidt, *Math. Ann.* **63**, 433 (1907).
- [82] A. Ekert and P. L. Knight, *Am. J. Phys.* **63**, 415 (1995).
- [83] H. Araki and E. H. Lieb, in *Inequalities* (Springer Berlin Heidelberg, Berlin, Heidelberg, 2002) pp. 47–57.
- [84] E. Boukobza and D. J. Tannor, *Phys. Rev. A* **71**, 063821 (2005).
- [85] M. A. Fasihi and B. Mojaveri, *Quantum Inf. Process.* **18**, 75 (2019).
- [86] M. Yönaç, T. Yu, and J. H. Eberly, *J. Phys. B* **39**, S621 (2006).
- [87] S. V. Prants, M. Y. Uleysky, and V. Y. Argonov, *Phys. Rev. A* **73**, 023807 (2006).
- [88] L. Tan, Y.-Q. Zhang, and Z.-H. Zhu, *Chin. Phys. B* **20**, 070303 (2011).
- [89] J. Cheng, X. Chen, and C.-J. Shan, *Int. J. Theor. Phys.* **57**, 1823 (2018).
- [90] V. Bartzis, *Phys. A: Stat. Mech. Appl.* **180**, 428 (1992).
- [91] S. Yang, Y. Ya-Ping, and C. Hong, *Chin. Phys. Lett.* **23**, 1136 (2006).
- [92] Y.-H. Hu and Y.-G. Tan, *Phys. Scr.* **89**, 075103 (2014).
- [93] M. Wilkens and P. Meystre, *Opt. Commun.* **94**, 66 (1992).
- [94] G. M. Palma and F. S. Persico, *EuroPhys. Lett. (EPL)* **17**, 207 (1992).
- [95] W. Ren, J. D. Cresser, and H. J. Carmichael, *Phys. Rev. A* **46**, 7162 (1992).
- [96] S. Xie, F. Jia, and Y. Yang, *Opt. Commun.* **282**, 2642 (2009).
- [97] M. Abdalla, M. Abdel-Aty, and A.-S. Obada, *Phys. A: Stat. Mech. Appl.* **326**, 203 (2003).
- [98] S. Abdel-Khalek, M. Quthami, and M. M. Ahmed, *Opt. Rev.* **22**, 25 (2015).
- [99] P. Knight and P. Radmore, *Phys. Lett. A* **90**, 342 (1982).
- [100] T. von Foerster, *J. Phys. A* **8**, 95 (1975).

- [101] B. Buck and C. Sukumar, [Phys. Lett. A **81**, 132 \(1981\)](#).
- [102] C. Sukumar and B. Buck, [Phys. Lett. A **83**, 211 \(1981\)](#).
- [103] A. Klimov and S. Chumakov, [Phys. Lett. A **264**, 100 \(1999\)](#).
- [104] S. Scheel, J. Eisert, P. L. Knight, and M. B. Plenio, [J. Mod. Opt. **50**, 881 \(2003\)](#).
- [105] J. Gea-Banacloche, [Opt. Commun. **88**, 531 \(1992\)](#).
- [106] K. Zaheer and M. S. Zubairy, [Phys. Rev. A **39**, 2000 \(1989\)](#).
- [107] D. Jonathan, K. Furuya, and A. Vidiella-Barranco, [J. Mod. Opt. **46**, 1697 \(1999\)](#).